First publ. in: Europhysics Letters 58 (2002), 6, pp. 906-911

Direct correlation of Cr $3d$ orbital polarization and O K-edge X-ray magnetic circular dichroism of epitaxial CrO_2 films

E. Goering[1], A. Bayer[3], S. Gold[1], G. Schütz[1], M. Rabe[2], U. Rüdiger[2] and G. Güntherodt[2]

[1] *MPI für Metallforschung - Heisenbergstrasse 1, 70569 Stuttgart, Germany*
[2] *II. Physikalisches Institut, Rheinisch-Westfälische Technische Hochschule Aachen 52056 Aachen, Germany*
[3] *Institut für Umweltphysik, Universität Heidelberg - 69120 Heidelberg, Germany*

(received 14 January 2002; accepted in final form 28 March 2002)

PACS. 78.20.Ls – Magnetooptical effects.
PACS. 75.30.Gw – Magnetic anisotropy.
PACS. 78.70.Dm – X-ray absorption spectra.

Abstract. – The role of delocalization and hybridization in complex magnetic oxides has been investigated by magnetic oxygen K-edge absorption of circular polarized soft X-rays in epitaxial grown CrO_2 as a function of the azimuthal angle at grazing incidence. Unusual strong variations in the typically small X-ray magnetic circular dichroism (XMCD) signal have been observed. Those angular dependencies of the typical CrO_2 oxygen K-edge XMCD signal could be quantitatively interpreted in terms of an induced anisotropic Cr $3d$ orbital magnetism for different spectral regions of the unoccupied density of states. The results strongly suggest a delocalized non-ionic magnetic behavior of the conduction electrons.

Introduction. – Recently, half-metallic CrO_2 has attracted a revived research interest due to its remarkable high spin polarization at the Fermi level, theoretically predicted to 100% [1–4] and verified by superconducting tunneling spectroscopy at 1.8 K [5,6] and spin-polarized photoemission spectroscopy at $T = 293$ K [7]. The reason for this revival are potential applications of magnetoelectronic and spintronics devices on the basis of half-metallic ferromagnets such as CrO_2 due to its intrinsic high degree of spin polarization [8] and Curie temperature well above RT. The oxygen-mediated magnetic coupling and the half-metallic nature are challenging tasks for theoretical investigations, originated by the presence of oxygen-hybridization, double-exchange, self-doping and correlation effects [2]. CrO_2 has a magnetic moment of 2 μ_B/Cr-ion, which is consistent with a fully spin-polarized band structure and also with an ionic $3d^2$ configuration. Therefore, transition-metal-oxide absorption spectra have been theoretically modeled in a full ionic ligand field approach [9]. Due to the metastable nature of the CrO_2 surface at $T = 293$ K and ambient atmosphere, spectroscopic and surface-sensitive measurements have been a challenging problem in the past. Nevertheless, epitaxially grown thin CrO_2 (100) films could be prepared, showing a magnetic easy axis along the in-plane c-axis for an unstrained sample [10,11].

Experimental. – CrO_2 crystallizes in a rutile structure with two equivalent a-axes (4.421 Å) and a shorter c-axis (2.916 Å) [12]. The CrO_2 films investigated have been epitaxially grown on isostructural TiO_2 substrates by a chemical vapor deposition technique CVD [13] with a sample thickness of $d \approx 100$ nm. The samples are (100)-oriented with in-plane a- and c-axis as indicated in the inset of fig. 1b. A Curie temperature of $T_c \approx 385$ K has been determined. Nearly no surface contamination of Cr_2O_3 is present [14,15] which was also reported by other groups [16]. Further details of the sample growth and characterization have been discussed elsewhere [17].

All spectra were recorded in total electron yield mode (TEY) at the bending-magnet-beamline PM I at BESSY II with an energy resolution of about $E/\Delta E = 2000$ and a degree of circular polarization of 95%. The spectra were acquired in an applied magnetic field of ± 5 kOe (flipped at each data point). The magnetization reversal of the sample has been checked with *in situ* XMCD Cr L_3-magnetization curves [18]. The samples have been saturated at a magnetic field of 0.5 kOe (2.5 kOe) along the in-plane magnetic easy c-axis (hard a-axis). All spectra have been measured at a temperature of $T = 80$ K. A careful background subtraction and edge normalization method have been applied [19]. No smoothing or further data manipulation have been performed. Details of the experimental setup and data analysis have been published elsewhere [19].

The experimental geometry is displayed in the inset of fig. 1b. XMCD spectra were taken with fixed grazing incidence ($\phi = 60°$) and the sample was rotated by the azimuthal angle ϑ around the surface normal.

Results. – Figure 1a shows normalized X-ray absorption spectra (XAS) for enhanced a- and c-axis projections of the photon k-vector and fig. 1b the corresponding XMCD spectra. A narrow feature near threshold at around 529 eV as well as a second feature approximately 3 eV above and of 3 eV width have been observed. This is consistent with a recent LSDA+U calculation by Korotin *et al.*, where the first narrow peak is identified as t_{2g}-majority states, while the second broad structure is a mixture of e_g-majority as well as t_{2g}- and e_g-minority states [2,16].

The azimuthal angular dependence of the O K-edge absorption (fig. 1a) exhibits very strong changes in the XAS signal using circular polarized light, which probes two perpendicular non-magnetic contributions of O K-edge XAS, being in contrast to previously published results of Stagarescu *et al.* using linear polarized light [16]. For the photon k-vector along the c-axis only in-plane electrical field components of the (a,a)-plane are present and dipolar allowed $2p_a$ contributions are probed. This is nearly the case (exactly for $\phi = 90°$) for the k-vector parallel to the c-axis in fig. 1a. After an azimuthal rotation by 90° the k-vector is oriented nearly parallel to the a-axis and electrical field components along the a- and the c-axis are present. Therefore only dipolar-allowed $2p_a$ and $2p_c$ contributions are probed. This is the reason why (a,a)-plane oriented states near the Fermi energy are only reduced to the half of its maximum for $\vec{k} || \vec{a}$ and not to zero as previously reported for linear polarized light [16]. We have checked and interpreted the observed XAS angular dependence quantitatively [20] similar to Stagarescu *et al.* (not shown) [16]. As a proof, two different ϕ scans with fixed azimuth angle corresponding to a rotation along the in-plane a- and c-axis (not shown) have been performed. For the in-plane c-axis rotation, with the photon k-vector oriented within the crystallographic (a,a)-plane, no changes of the XAS spectra could be observed. While for the other scan with rotation along the in-plane a-axis, the photon k-vector varies from c- to a-axis projections similar to the grazing incidence azimuthal scans shown in fig. 1a. Analogous changes in the XAS spectra could be observed. This provides strong evidence that all observed variations are related to crystallographic projections. Figure 1b shows the corresponding CrO_2 XMCD spectra for a fixed grazing incidence condition ($\phi = 60°$) with a variation of the azimuthal

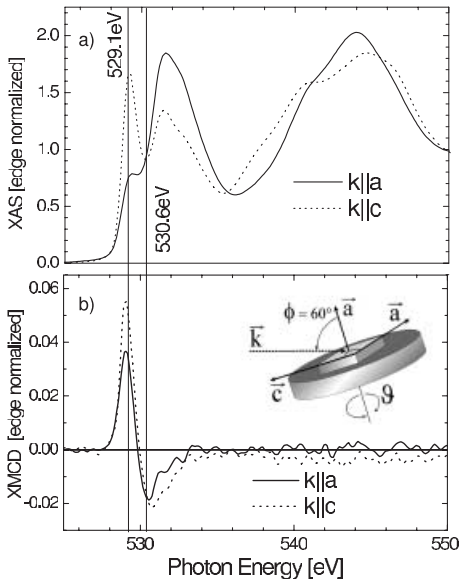

Fig. 1

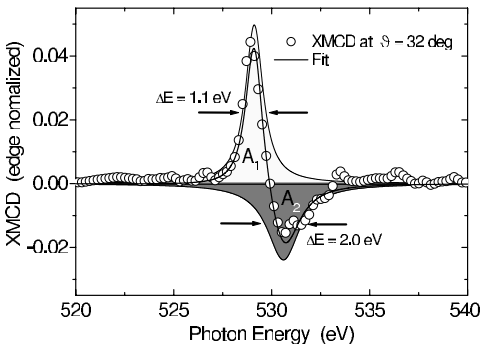

Fig. 2

Fig. 1 – a) CrO_2 O K-edge XAS and b) XMCD signal at an applied magnetic field of 5 kOe for two different azimuthal angles ($\vartheta = 0°$ and $\vartheta = 90°$) and fixed $\phi = 60°$; the inset shows the experimental geometry of the sample relative to the incoming photon beam.

Fig. 2 – O K-edge XMCD signal (○) and the fit result (—) as a sum of two Lorentzian contributions of opposite sign (grey shaded areas).

angle ϑ. A narrow positive peak near the threshold and a broader structure with negative sign at slightly higher energies are present, which are on average similar to previously performed XMCD measurements on powder samples [21]. We have measured at different angles (ϑ) but only extremal projections are shown to enhance visibility. The first narrow positive peak at 529.1 eV has a stronger angular dependence whereas the second negative peak at about 530.1 eV shows a less pronounced angular dependence. For a quantitative analysis the O K-edge XMCD spectra have been fitted by two different Lorentzian curves with fixed energy positions of 529.1 eV (530.6 eV) and peak width of 1.1 eV (2.0 eV). The energy separation of both peaks corresponds with the DOS calculated by Korotin *et al.* [2]. Figure 2 shows a representative fit result with two Lorentzian lines and the experimental XMCD data for an intermediate angle of ($\vartheta = 32°$). A similar approximation with the same quality has been achieved for the other measured O K-edge spectra. The resulting fitted areas below each Lorentzian line are shown in fig. 4 below. Variations with angle are observed. The first narrow peak (A_1) exhibits a stronger angular dependence than the second broad peak (A_2).

Discussion. – As recently shown for a polycrystalline highly textured CrO_2 (100) sample [15] as well as for an epitaxially grown CrO_2 (100) thin film [14], two orbital contributions could be extracted from Cr $L_{2,3}$ XMCD spectra using the so-called moment analysis technique [22, 23], originally used for the interpretation of pure $3d$ metal XMCD spectra [24–26]. Cr $L_{2,3}$ XMCD data has been previously fitted (fig. 3b) by superposition of two sets of ground-state moments [14] corresponding to the projected DOS reproduced from ref. [2] in fig. 3a. All spectral Cr $L_{2,3}$ XMCD features could be reproduced by this fitting procedure. Fit results of each orbital contribution ($\langle L\rangle_1$ and $\langle L\rangle_2$) are presented in figs. 4 and 5a.

For a quantitative comparison of Cr $L_{2,3}$- and O K-edge spectra the Cr $L_{2,3}$ projected

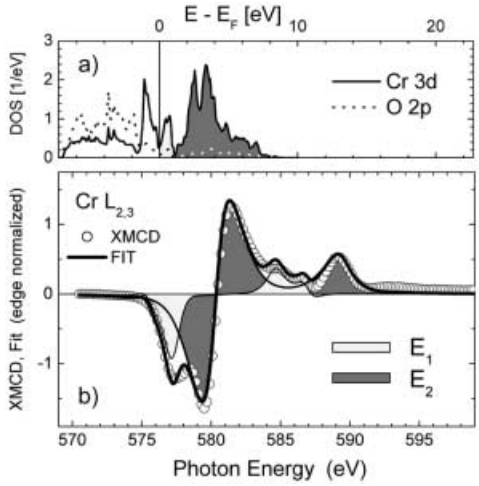

Fig. 3

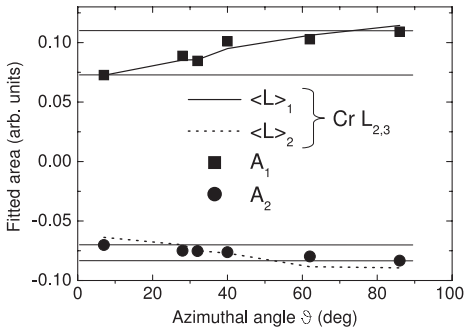

Fig. 4

Fig. 3 – a) Cr 3*d* (—) and O 2*p* (···) DOS from ref. [2]; b) Cr $L_{2,3}$ XMCD (○) and moment analysis fit result (—) corresponding to two different energy contributions E_1 and E_2 [14].

Fig. 4 – Fit result of the angular dependence of the O *K*-edge XMCD for the two different Lorentzian lines A_1 (■) and A_2 (●) (see fig. 2) in comparison to scaled and shifted Cr $L_{2,3}$ orbital contributions $\langle L\rangle_1$ (—) and $\langle L\rangle_2$ (···).

orbital moments [14] have been scaled for both contributions with the same factor, held fixed for both energies and shifted apart from the *x*-axis with an offset of +0.08 (−0.05). The resulting scaled and shifted Cr 3*d* orbital projections $\langle L\rangle_1$ ($\langle L\rangle_2$) are shown in fig. 4 as straight (dotted) lines.

The observed angular dependence in the O *K*-edge XMCD and Cr $L_{2,3}$ orbital projections show exactly the same behavior. For further clarification additionally absolute values of angular-dependent differences have been plotted for both energies for the Cr $L_{2,3}$ orbital projections (fig. 5a) [14] and the O *K*-edge XMCD (fig. 5b). Experimental values have been mirrored along the horizontal and vertical axes to give a full 360° polar plot. A clear one-to-one relationship between the O *K*-edge XMCD and the Cr $L_{2,3}$ orbital projections can been identified. Due to the missing spin-orbit coupling in the oxygen 1*s* shell, spin contributions of the O *K*-edge XMCD are cancelled out and the XMCD signal is theoretically interpreted as a representation of projected orbital contributions of unoccupied *p*-states [27, 28]. In the model of Bruno [29], a residual orbital moment is a result of the 3*d* spin-orbit coupling. In other words, the spin-orbit interaction leads to a small energy splitting of opposite m_l contributions to eigenstates of the crystal field operator. In a band, structure–related picture this splitting is present for the eigenstates of CrO_2 and, therefore, also observable at O 2*p* projections with different O 2*p* m_l contributions.

The comparison of O *K*-edge XMCD and Cr $L_{2,3}$ orbital contributions shows a strong similarity. Both the O *K*- and Cr $L_{2,3}$-edge spectra can be quantitatively interpreted as a sum of only two different energy contributions, separated by 1.5 eV (2.6 eV) and corresponding linewidths of 1.1 and 2.0 eV (1.0 and 2.6 eV), respectively. The energy splitting and effective linewidth of the second broad peak are reduced for O *K*-edge XMCD spectra. This effect can be explained by a strong decrease of O 2*p* admixture at higher energies, which is observable in the band structure calculation of Korotin *et al.* [2]. This effect cuts off higher-energy contributions and results in those small differences in the observed linewidth.

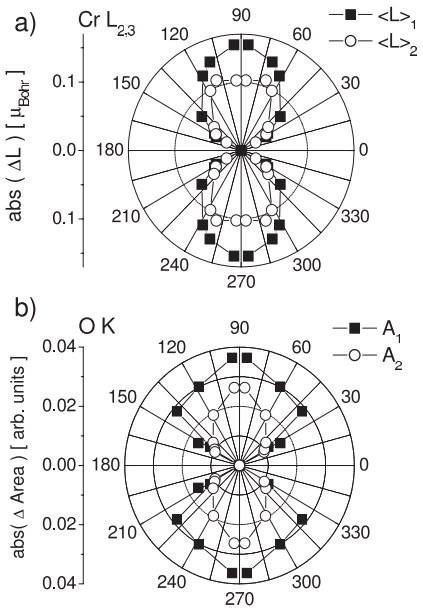

Fig. 5 – a) Sum rule related Cr $L_{2,3}$ differences of projected orbital moment contributions ΔL at the threshold energy $\langle L\rangle_1$ and 2.6 eV above $\langle L\rangle_2$ as a function of the azimuthal angle ϑ. b) O K-edge XMCD fitted area ΔA at the threshold energy(A_1) and 1.7eV above (A_2).

All the observed similarities strongly support that a band-structure–related description of the ferromagnetic state of CrO_2 is more appropriate compared to a localized ionic moment picture with a simple Cr $3d^2$ configuration. Similar correspondence between non-magnetic XAS and LDA-DOS calculations has been achieved for other light transition metal oxides like VO_2 and V_2O_3 [30–32]. The application of sum rules for the Cr $L_{2,3}$ spectra leads to a spin moment of $1.9\mu_B$ only by a proper quantitative hybridization correction [14]. For a 100 nm thick CrO_2 (100) film, it is unlikely that the observed twofold magnetocrystalline anisotropies are related to strain-induced effects due to the presence of a lattice mismatch between CrO_2 and the TiO_2 substrate. Additionally, the average sampling depth for XMCD in TEY mode of 2–5 nm [33] leads to an enhanced surface-sensitive measurement, where the lattice mismatch-induced strain plays no role.

Summary. – The lineshape and the azimuthal angular variations of the O K-edge XMCD could be quantitatively interpreted as hybridization-related $2p$ orbital magnetic moments with a clear correspondence between O K-edge XMCD and Cr $3d$ projected orbital moments. Two different peaks of opposite sign are identified as pure t_{2g}-majority and a mixture of e_g-majority as well as t_{2g}- and e_g-minority states near the Fermi edge, which is consistent with recent band structure calculations [2]. Our results give strong evidence that a band-type related description of CrO_2 including pronounced hybridization effects is necessary for describing the magnetic properties of CrO_2 such as the reduced Cr spin moment and the O K-edge XMCD. An ionic picture and a pure Cr $3d^2$ configuration could not simply explain O K-edge XMCD results which was also suggested by Korotin *et al.* [2] due to the presence of a dispersing nearly pure O $2p$-like band which leads to the so-called oxygen self-doping effects and a corresponding double-exchange description of the metallic behavior of CrO_2.

We would like to express our gratitude to the beamline staff and all the other helpful people at BESSY II and to A. Peter, F. Weigand, J. Geissler and R. Eder for fruitful discussions. This work was supported by the DFG Forschergruppe Augsburg, Contract number SCHU 964/4-5 and by the German Federal Ministry of Education and Research (BMBF) grant No. FKZ O5K51PAA/7.

REFERENCES

[1] Schwarz K., *J. Phys. F*, **16** (1986) L211.
[2] Korotin M. A., Anisimov V. I., Khomskii D. I. and Sawatzky G. A., *Phys. Rev. Lett.*, **80** (1998) 4305.
[3] Lewis S. P., Allen P. B. and Sasaki T., *Phys. Rev. B*, **55** (1997) 10253.
[4] Mazin I. I., Singh D. J. and Ambrosch-Draxl C., *Phys. Rev. B*, **85** (1999) 6220.
[5] Soulen R. J. *et al.*, *Science*, **282** (1998) 85.
[6] Ji Y. *et al.*, *Phys. Rev. Lett.*, **86** (2000) 5585.
[7] Dedkov Yu. S., Fonine M., König C., Rüdiger U. and Güntherodt G., submitted to *Appl. Phys. Lett.* (2002).
[8] Julliére M., *Phys. Lett. A*, **54** (1975) 225.
[9] de Groot F. M. F. *et al.*, *Phys. Rev. B*, **40** 5715 (1989); **42** (1990) 5459.
[10] Li X. W., Gupta A. and Xiao G., *Appl. Phys. Lett.*, **75** (1999) 7134.
[11] Anguelouch A., Gupta A. and Xiao G., *IEEE Trans. Magn.*, **37** (2001) 2135.
[12] Porta P., Marezio M., Remeika J. P. and Dernier P. D., *Mater. Res. Bull.*, **7** (1972) 157.
[13] Ishibashi S., Namikawa T. and Satou M., *Mater. Res. Bull.*, **14** (1979) 51.
[14] Goering E. *et al.*, to be published in *Phys. Rev. Lett.* (2002).
[15] Goering E., Justen M., Geissler J., Rüdiger U., Rabe M., Güntherodt M. G. and Schütz G., *Appl. Phys. A*, **74** (2002) 747.
[16] Stagarescu C. B., Su X., Eastman D. E., Altmann K. N., Himpsel F. J. and Gupta A., *Phys. Rev. B*, **61** (2000) R9233.
[17] Rabe M. *et al.*, *J. Phys. Condens. Matter*, **14** (2002) 7.
[18] Goering E., Fuss A., Weber W., Will J. and Schütz G., *J. Appl. Phys.*, **88** (2000) 5920.
[19] Goering E., Gold S., Bayer A. and Schütz G., *J. Syncr. Radiat.*, **8** (2001) 434.
[20] Bayer A., to be published.
[21] Attenkofer K. and Schütz G., *J. Phys. IV*, **7** (1997) C2-459.
[22] Goering E., Gold S. and Schütz G., *J. Syncr. Radiat.*, **8** (2001) 422.
[23] Goering E., Ahlers D., Attenkofer K., Obermeier G., Horn S. and Schütz G., *J. Syncr. Radiat.*, **6** (1999) 537.
[24] van der Laan G., *J. Phys. Condens. Matter*, **9** (1997) L259.
[25] van der Laan G., *Phys. Rev. B*, **55** (1997) 8086.
[26] O'Brien W. L. *et al.*, *J. Appl. Phys.*, **76** (1994) 6462.
[27] Ebert H., *Rep. Prog. Phys.*, **59** (1996) 1665.
[28] Igarashi J. and Hirai K., *Phys. Rev. B*, **50** (1994) 17820.
[29] Bruno P., *Phys. Rev. B*, **39** (1989) 865.
[30] Goering E., Müller O., Klemm M., denBoer M. L. and Horn S., *Philos. Mag. B*, **75** (1997) 229.
[31] Müller O. *et al.*, *J. Phys. IV*, **7** (1997) C2-533; *Phys. Rev. B*, **56** (1997) 15056.
[32] Eyert V., Horny R., Höck K. H. and Horn S., *J. Phys. Condens. Matter*, **12** (2000) 4923.
[33] Nakajima R., Stöhr J. and Idzerda Y. U., *Phys. Rev. B*, **59** (1999) 6421.